Nuclear Instruments and Methods in Physics Research A 818 (2016) 68–75

Contents lists available at ScienceDirect

Nuclear Instruments and Methods in Physics Research A

journal homepage: www.elsevier.com/locate/nima

A de-noising algorithm to improve SNR of segmented gamma scanner for spectrum analysis

Huailiang Li [a,*], Xianguo Tuo [a,b], Rui Shi [b], Jinzhao Zhang [a], Mark Julian Henderson [a], Jérémie Courtois [c], Minhao Yan [c]

[a] Fundamental Science on Nuclear Wastes and Environmental Safety Laboratory, Southwest University of Science and Technology, Mianyang 621010, China
[b] State Key Laboratory of Geohazard Prevention & Geoenvironmental Protection, Chengdu University of Technology, Chengdu 610059, China
[c] State Key Laboratory Cultivation Base for Nonmetal Composites and Functional Materials, Southwest University of Science and Technology, Mianyang 621010, China

ARTICLE INFO

Article history:
Received 23 July 2015
Received in revised form
2 February 2016
Accepted 15 February 2016
Available online 23 February 2016

Keywords:
γ-spectrum analysis
Shift-invariant wavelet transform
De-noising

ABSTRACT

An improved threshold shift-invariant wavelet transform de-noising algorithm for high-resolution gamma-ray spectroscopy is proposed to optimize the threshold function of wavelet transforms and reduce signal resulting from pseudo-Gibbs artificial fluctuations. This algorithm was applied to a segmented gamma scanning system with large samples in which high continuum levels caused by Compton scattering are routinely encountered. De-noising data from the gamma ray spectrum measured by segmented gamma scanning system with improved, shift-invariant and traditional wavelet transform algorithms were all evaluated. The improved wavelet transform method generated significantly enhanced performance of the figure of merit, the root mean square error, the peak area, and the sample attenuation correction in the segmented gamma scanning system assays. We also found that the gamma energy spectrum can be viewed as a low frequency signal as well as high frequency noise superposition by the spectrum analysis. Moreover, a smoothed spectrum can be appropriate for straightforward automated quantitative analysis.

1. Introduction

High-resolution gamma-ray spectroscopy (HRGS) is routinely used in segmented gamma scanning (SGS) measurements, where it uses the full-energy response to determine the quantity of the gamma-ray emitting material within a sample, and also provides the capability of identifying radionuclides from complex gamma-ray spectra [1–4]. In an assay with large samples, e.g. 200 L drums containing medium and high-density matrices, continuum build-up caused by Compton scattering in the sample can substantially reduce the signal-to-noise (SNR) ratio of the full-energy measurement. The quantity and location of gamma ray emitting material also influences the signal quality [5–8].

By improving measurement accuracy to determine the radioactive materials and reducing the statistical fluctuations, the wavelet transform processing of gamma-ray spectroscopy offers an improved de-noising effect [9–12]. Wavelet transform has been used in the field of image de-noising with promising results. Kingsbury proposed the dual-tree complex wavelets transform (CWT) with perfect reconstruction and good filter characteristics that yielded an attractive performance for image processing, such as reduced noise [13]. Starck et al. introduced a simple interpolation in Fourier space and used a ridgelet transform as a component step, which implemented curvelet subbands by using a filter bank of trous wavelet filters [14]. Blu and Luisier proposed a new approach for image de-noising, armed with Stein unbiased risk estimator and linear expansion of thresholds (LET) principle (SURE-LET), to solve linear system of equations in a fast and efficient manner [15]. You Xinge et al. suggested an image de-noising method based on non-separable wavelet filter banks and 2D-principal components analysis (2D-PCA) without a complex de-noising preprocessing, which achieved both good visual quality and a high peak signal-to-noise ratio for the noise reduction images [16]. In this study, an improved threshold shift-invariant wavelet de-noising HRGS method is presented. This method maintains the measurement spectrum quality, improves the

Abbreviations: WT, wavelet transform; S-I WT, shift-invariant wavelet transform; CWT, complex wavelets transform; HRGS, high-resolution gamma-ray spectroscopy; SGS, segmented gamma scanning; SNR, signal-to-noise ratio; AC, attenuation coefficient; FOM, figure of merit; RMSE, root mean square error; DWT, discrete-time wavelet transform; ABS, acrylonitrile butadiene styrene plastics.

* Corresponding author at: Southwest University of Science and Technology, Fundamental Science on Nuclear Wastes and Environmental Safety Laboratory, Chengdu 621010, China. Tel.: +86 13679023291.
E-mail address: li-huai-liang@163.com (H. Li).

http://dx.doi.org/10.1016/j.nima.2016.02.047
0168-9002/

performance of figure of merit (FOM) and attenuation coefficient (AC) correction, and reduces root mean square error (RMSE) in SGS assays, which generates basic data for radionuclide identification and quantification.

2. Materials and methods

2.1. RMSE, FOM, peak area, and sample AC

For gamma-ray spectra, improvements in RMSE, FOM, peak areas, and sample attenuation correction were measured before and after the application of a de-noising algorithm. A lower RMSE indicated better reduction of noise as well as decreased deformation of noise-suppressed data. RMSE formula is described as follows:

$$\mathrm{RMSE}=\sqrt{\frac{\sum_{i=1}^{n}(y_i-\hat{y}_i)^2}{n}} \tag{1}$$

where $n=$ number of measurements, $y_i=$truth value, and $\hat{y}_i=$measured value of y_i.

FOM is a commonly used criterion to evaluate the device detection capabilities of weak γ peaks. FOM is a function of the measuring radioactivity counting time, which corresponds to the least relative standard deviation. The higher the FOM (denoted as Q), the less time it takes to measure the activity. On the contrary, the lower the quality factor with Q, the more time required for measurement. It is defined as:

$$Q=\nu^2 n_0^2/\left(\sqrt{n_0+n_b}+\sqrt{n_b}\right)^2 \tag{2}$$

where $n_0=$sample net peak area, $n_b=$background net peak area (as Compton scattering continuum counts), $\nu=$relative standard error of n_0 [17], $\nu=(\mathrm{mean}(n_0)-n_0)/\mathrm{sqrt}(n_0)$, and it characterizes the fitting average relative error.

The parameters n_0, n_b, and ν were obtained by using the method described by Covell to calculate the peak area [18]. The sample AC in SGS determines the quality of the peak count accumulation. The AC was obtained by comparing measured peak area with the theoretical value shown in formula (3),

$$\mathrm{AC}=\frac{\ln I_o-\ln I}{\Delta x} \tag{3}$$

where $I_o=$ intensity of incident gamma ray, $I=$intensity of outgoing gamma ray, and $\Delta x=$material thickness. The details for this calculation method can be found in [2].

2.2. De-noising algorithms

2.2.1. Traditional wavelet transform

The wavelet transform is an integral transform of the 'time-frequency' analysis of signals, and can be used in various signal-processing applications. In this study, we used discrete-time wavelet transform (DWT) that uses the mother wavelet function φ to decompose the spectra into a multilevel set of approximations. The DWT has vertical, horizontal and diagonal wavelet coefficients c^L, where $L=1,2,3\cdots$, and L gives the level of decomposition. A more detailed description of the wavelet transform and its properties are provided by Donoho [19].

The selection of an appropriate mother wavelet was based both on theoretical criteria and experimental tests. Firstly, the mother wavelet should be suitable for discrete analysis. Daubechies (db) wavelets and symlets are orthogonal and compactly supported wavelets with similar properties, and are typically used in discrete analysis applications using a fast algorithm for DWT. Secondly, the order of the mother wavelet had to be high enough to result in efficient smoothing of the irregular parts of the spectrum. After a systematic trial-and-error study, the wavelet base function, sym8, was selected as the mother wavelet for smoothing purposes of all analyzed measured spectra [19].

In general, L, the level of wavelet decomposition is an important parameter for successful application of an algorithm. More specifically, different values of L have to be introduced in order to compensate for a considerable decrease of spectrum statistics as the gamma-ray energy increases. After a systematic trial-and-error study and combining with Wei W and Tie C's selection method [20,21], $L=5$ was selected as the level for smoothing purposes of all analyzed and measured spectra.

DWT is most frequently used in gamma-ray spectral analysis for computing appropriate threshold values for wavelet coefficients, i.e., 'thresholding.' It is assumed that the wavelet coefficients of noisy samples with values lower than a particular threshold value λ can be cancelled, which leads to noise reduction in the image domain. When the remaining coefficients are unaffected, it is referred to as hard thresholding:

$$\hat{c}=\begin{cases} c & |c|\geq\lambda \\ 0 & |c|<\lambda \end{cases} \tag{4}$$

where $\hat{c}=$wavelet coefficient. Another common type of thresholding technique is soft threshold, defined as:

$$\hat{c}=\begin{cases} \mathrm{sign}(c)\cdot\left[|c|-\lambda\right] & |c|\geq\lambda \\ 0 & |c|<\lambda \end{cases} \tag{5}$$

Soft threshold yields a better smoothing result, whereas hard threshold effectively preserves the slope edge.

2.2.2. Improved WT algorithms

The most important part of the de-noising algorithm is an estimation of the optimal threshold value. When the threshold value is too low, the noise reduction is inefficient. On the other hand, details of image information can be lost when the threshold value is too high. In this work, we adopted one of the most frequently used estimation algorithms [13], which is also the universal threshold (as an improved WT de-noising), defined as:

$$\lambda=\sigma\sqrt{2\log_2(N)} \tag{6}$$

where $N=$channel number of the spectrum and $\sigma=$standard deviation of noise. The universal threshold was estimated by using the Donoho and Johnstone theorem as the statistical median MAD of detailed wavelet coefficients, c^L, and from the first decomposition level divided by the constant 0.6745 [13]. This threshold was then applied to all detailed wavelet coefficients of each decomposition level:

$$\sigma=\frac{\mathrm{MAD}(c^L)}{0.6745} \tag{7}$$

where MAD$=$ estimated median value of absolute value of noise wavelet packet high frequency sub-band coefficients. In addition to the standard de-noising technique operating with the threshold, we used a protocol applied to the wavelet coefficients.

We found that the gamma energy spectrum can be viewed as a low frequency signal and high frequency noise superposition by the spectrum analysis. The high frequency noise signal is similar to white noise. If $\hat{f}(i)$ and $f(i)$ denoted the measured unwanted noisy and underlying required data (i.e. noiseless data) respectively, and $n(i)$ denoted the noise and i the channel of the spectra, then,

$$\hat{f}(i)=f(i)+n(i) \tag{8}$$

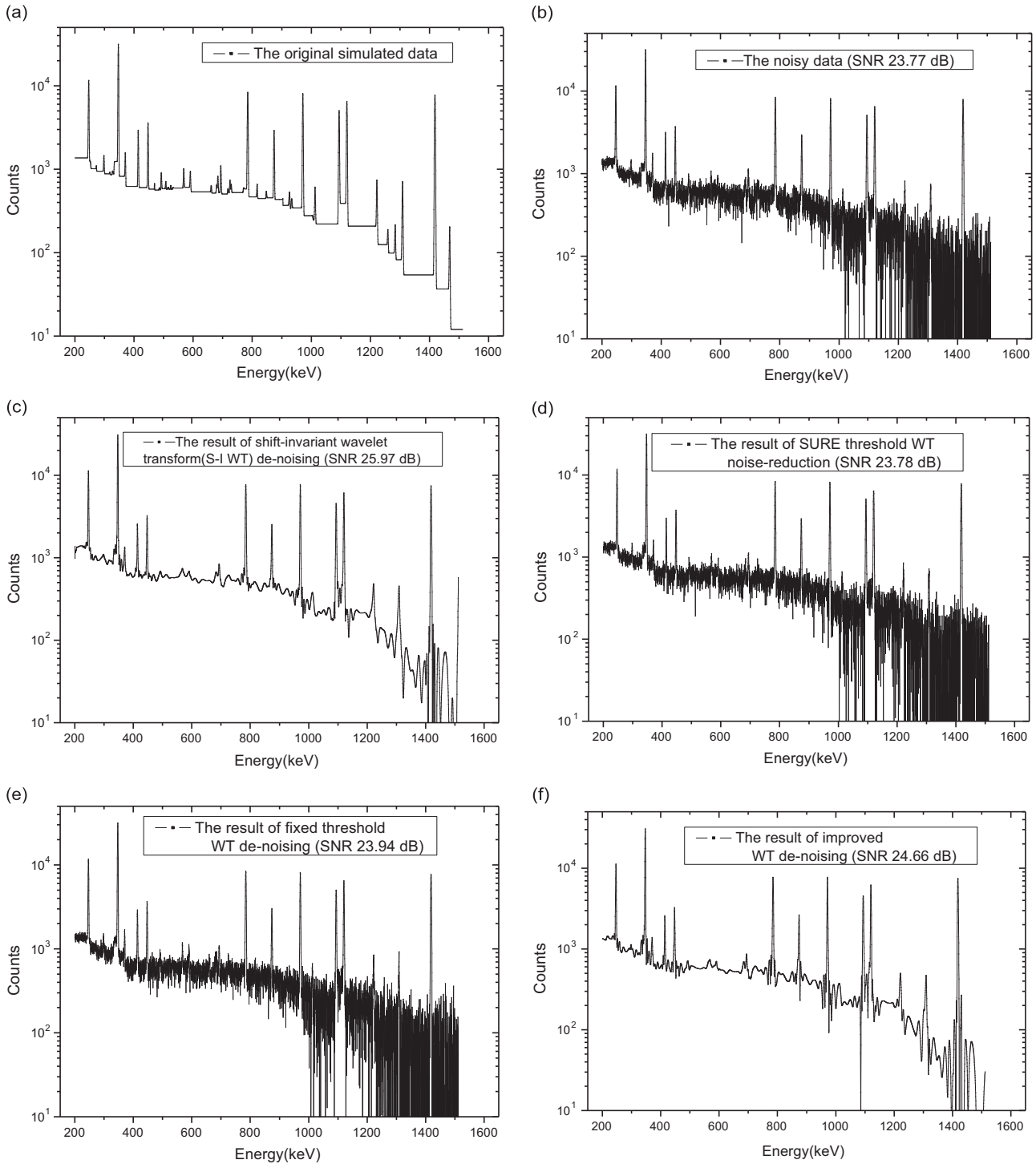

Fig. 1. (a) The original simulated data, (b) The noisy data (SNR 23.77 dB), (c) The result of shift-invariant wavelet transform (S-I WT) de-noising (SNR 25.97 dB), (d) The result of SURE threshold WT noise-reduction (SNR 23.78 dB), (e) The result of fixed threshold WT de-noising (SNR 23.94 dB), and. (f) The result of improved WT de-noising (SNR 24.66 dB).

The root mean square (RMS) of the spectrum can be obtained using the following formula:

$$\mathrm{RMS}[f(i)] = \sqrt{\sum_{i=1}^{N} f(i)^2/N} \tag{9}$$

The required data has no relationship to the noise, and the noise is Gaussian with a standard deviation of σ. We may express Eq. (8) using the results in Eq. (10) and Eq. (11) as:

$$\mathrm{RMS}\left[\hat{f}(i)\right]^2 = \mathrm{RMS}[f(i)]^2 + \mathrm{RMS}[n(i)]^2 \tag{10}$$

$$\mathrm{RMS}[f(i)] = \sqrt{\left|\mathrm{RMS}\left[\hat{f}(i)\right]^2 - \sigma^2\right|} \tag{11}$$

The method defined in Eq. (12) can be described as the multiplication of the universal threshold using the complex value of

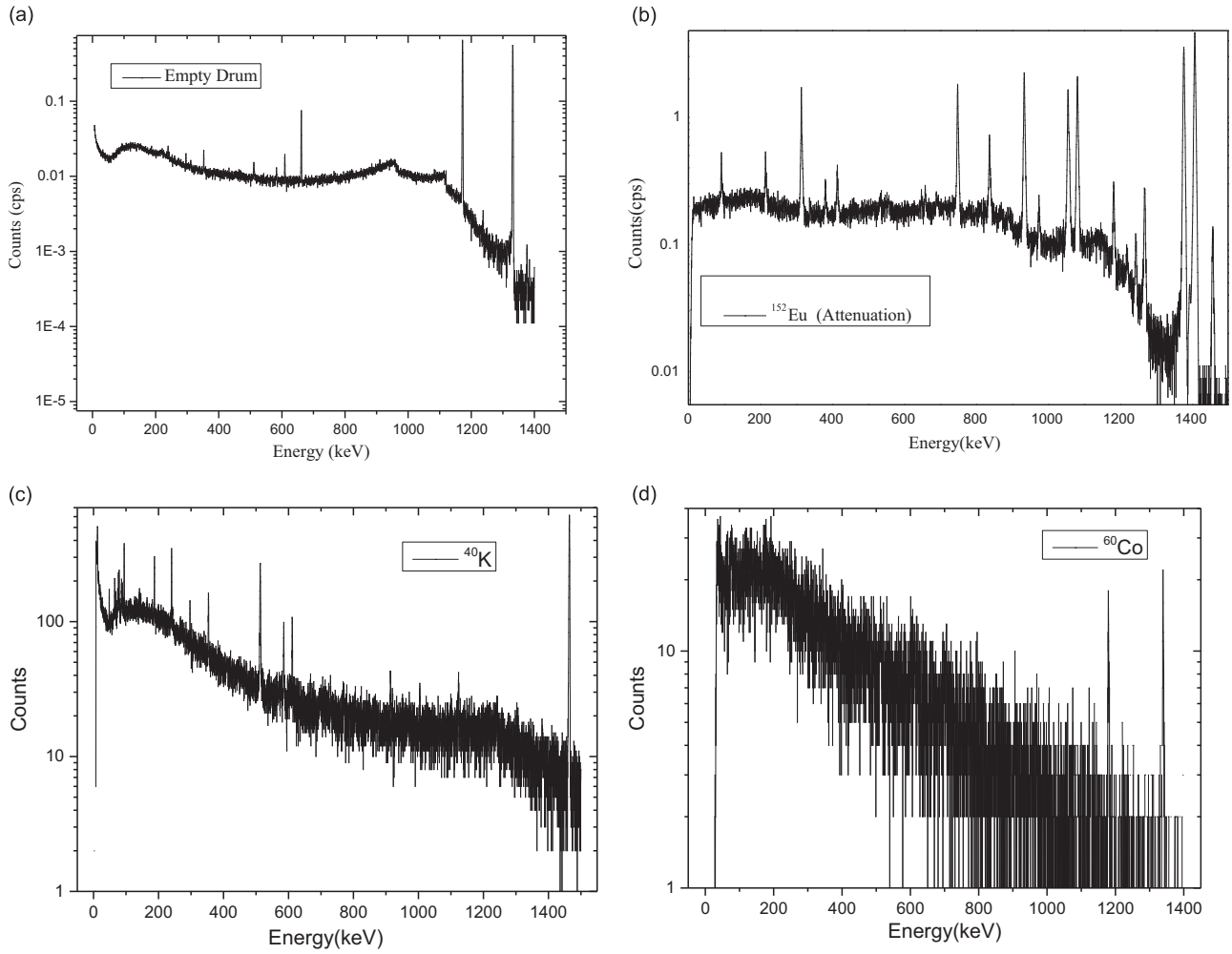

Fig. 2. The gamma ray spectrum of SGS system: (a) the spectrum of the transmission source ^{60}Co of the empty drum, (b) the spectrum of the transmission source ^{152}Eu, (c) and (d) show the emission spectrum of ^{40}K and ^{60}Co.

the 'attenuation' factor α, $0<\alpha<1$:

$$\lambda' = \alpha \cdot \sigma \cdot \sqrt{2 \cdot \log(N)} \tag{12}$$

where α can be obtained from the Eq. (13) and n in Eq. (13) is an arbitrary positive constant:

$$\alpha = \exp\left[\mathrm{RMS}\left[f(i)\right]/n\right] \tag{13}$$

We replaced α in Eq. (12) by Eq. (13), and obtained the following equation:

$$\lambda' = \exp\left[\sqrt{\mathrm{RMS}\left[\hat{f}(i)\right]^2 - \sigma^2}/n\right] \cdot \sigma \cdot \sqrt{2 \cdot \log(N)} \tag{14}$$

2.2.3. S-I WT algorithms

When the scale displacement-sampling interval is exponentially doubled, the orthogonal wavelet function set cannot be obtained from the perspective of multi-scale matching for the local structure of the signal characteristic. Therefore, the wavelet transform sometimes exhibits visual artifacts in the neighborhood of discontinuities [22,23]. The S-I WT de-noising method is an effective way for eliminating artificial signal oscillation that requires changing the arrangement order, and its specific steps are provided as follows:

Firstly, the time-domain translation operator was introduced. For signal x_t $(0 \le t \le N)$, S_h is defined as a shift operator with a cyclic shift quantity of h.

$$S_h(x_t) = x(t+h) \bmod N \tag{15}$$

Secondly, we selected the decomposition scale. Different frequency bands correspond to different scale decomposition. Finally, the spectrum signals corresponding to high and low frequency coefficients that dealt with the threshold were decomposed. The inverse shift spectrum was smoothed by the wavelet:

$$S_{-h}(x_t) = x(t-h) \bmod N \tag{16}$$

Finally, the artificial oscillation amplitude was minimized by selecting the optimal translation parameter h. However, when the spectrum contains a plurality of singular points, it is possible for a singular point shift quantity to be optimal and the singular point in a second, different shift quantity to be suboptimal. Therefore, for a complex spectrum, a range of translation was obtained through circulation translation, and the result was averaged in order to eliminate the phenomenon of oscillation.

3. Results and discussion

3.1. Simulated data

In this section, we evaluated the performance of our proposed algorithm on simulated data. The features are shown in Fig. 1(a)–(f):

We constructed the simulated spectrum using high purity germanium (HPGe) detector response function. The spectra that had to be modeled were: (i) full energy peak, (ii) single escape peak, (iii) double escape peak, (iv) incomplete charge collection (exponentially

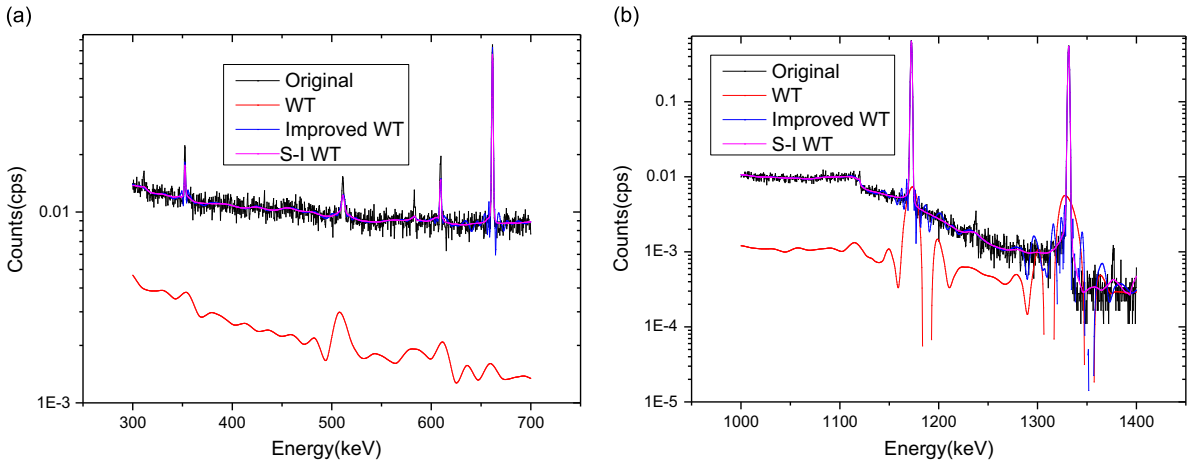

Fig. 3. De-noising: (a) 300–700 keV, and (b) 1000–1400 keV. Data from Fig. 2(a).

Table 1
Result of Fig. 2(a) de-noising.

Algorithm	Peak position (keV)	Net peak area (cps)	RMSE	AC of Fe	Relative error of AC
Original data	1173.24	2.6338	0	0.44810	0.04600
	1332.50	3.0449		0.43870	0.10630
WT	1173.24	0.8290	2.785e−2	6.23750	13.5610
	1332.50	0.7190		6.82150	16.2040
Improved WT	1173.24	2.6504	1.012e−3	0.42632	0.00481
	1332.50	3.0240		0.38022	0.04109
S-I WT	1173.24	2.6494	8.750e−4	0.42821	0.00040
	1332.50	3.0449		0.39558	0.00234

shaped) tail on the left side of the full energy peak, (v) uniform incomplete charge collection from zero to full energy, and (vi) Compton continuum including the multiple-scattering region. The main source of noise included instability of electronic components, physical statistical fluctuations and background effects.

As shown in Fig. 1(c), the S-I WT is characterized by significantly improved SNR. The de-noising effects of improved WT and S-I WT were better than SURE and fixed-threshold WT methods. Consequently, SURE and fixed-threshold WT methods were not considered hereafter.

3.2. Experimental results

Waste drums composed of Acrylonitrile Butadiene Styrene plastic (ABS) were used as a standard vessel for radionuclide measurements. The drum wall thickness was 1 mm.

Fig. 2 presents the original measurement of γ energy spectra of the SGS system. Fig. 2(a) shows the spectrum of the transmission source ^{60}Co of the empty drum, Fig. 2(b) the spectrum of the transmission source ^{152}Eu, which is a function of the sample quantity inside the waste drum, showing the spectra that were attenuated by ABS of ^{152}Eu (10 mCi). Fig. 2(c) and (d) show the emission spectrum of ^{40}K and ^{60}Co, respectively. All the spectra exhibited obvious statistical fluctuations, which increased with increasing sample quantity in the waste drum.

3.3. Analysis and discussion

As shown in Fig. 3 and Table 1, we used the empty drum as an original measurement energy spectrum. The signals at both sides of the peak were a pseudo-Gibbs phenomenon. These results demonstrated that using S-I WT de-noised spectra were in good agreement with the original data. The peak count rates were not significantly reduced, both sides of the full-energy peak and the small peaks of the low-energy regions were very smooth, and the noise was effectively removed. S-I WT not only de-noised the energy spectrum, but also distinguished the ^{214}Pb peak at 352 keV and the environmental background ^{214}Bi peak at 609 keV. This also illustrated that the translation invariant wavelet transform effectively detected weak signals.

Table 2
The peaks of ^{60}Co figure of merit (FOM).

Energy (keV)	Wavelet	S-I wavelet
1173.24	5.46E−04	5.83E−04
1332.50	5.01E−04	5.39E−04

The improved WT and S-I WT were characterized by significantly reduced RMSE. The de-noising effects of improved WT and S-I WT were better than that of WT. The peak areas were obtained using the calculation method described by Covell. Using this area, the AC relative error was calculated by using the improved WT, and the S-I WT was found to be smaller than the WT as well as the original. The precision was therefore enhanced by de-noising.

The spectral characteristic peaks of the original waveform and the waveform de-noised using WT had large relative errors, so the FOM of these spectra were not calculated. As shown in Table 2, we demonstrated that the S-I WT FOM increased compared with the improved WT. In addition, it took less time to calculate the activity using the algorithm. Consequently, the algorithm was more suitable for smoothing HRGS.

As shown in Fig. 4, the gamma-ray spectra of the ^{152}Eu transmission source characteristic peaks were distributed from low energy to high energy. After de-noising, all of the characteristic peaks were consistent with the original data using the S-I WT and the improved WT. Moreover, the peaks not only overcame statistical fluctuations with pseudo-Gibbs signals, but also demonstrated obvious de-noising effects.

As observed in Tables 3 and 4, and Fig. 4, the resulting trend is the same as Table 2. These results indicated that the RMSE and FOM of the gamma spectrum, which was de-noised using S-I WT and improved WT were better than that of the WT. For S-I WT, the ^{152}Eu characteristic peak FOMs had a greater value from low energy to high energy, except for 1085.78 keV and 1212.80 keV, which had too low counts. This indicated that the S-I WT method overcomes the disadvantages of the wavelet transform, and the high peaks and low count rate peaks produced better results than WT and improved WT. Additionally, the results showed that the

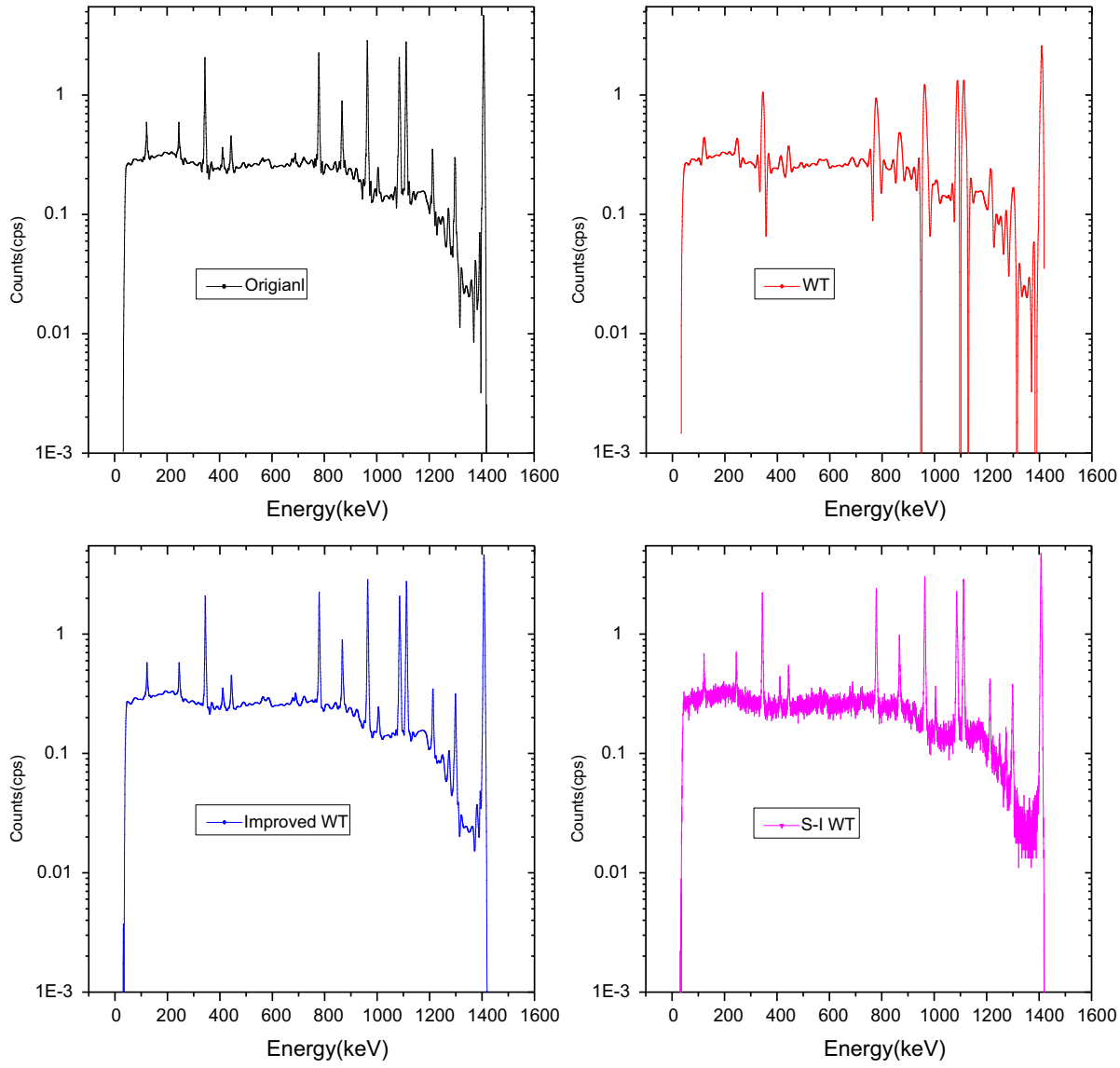

Fig. 4. Result of Fig. 2(b) de-noising.

Table 3
The RMSE of ^{152}Eu spectra de-noising.

De-noising algorithm	RMSE
S-I WT	0.01137
Improved WT	0.02836
WT	0.11726

Table 4
The peak of ^{152}Eu figure of merit.

Energy (keV)	Original data	S-I WT	Improved WT
121.78	1.55E−02	2.38E−02	1.57E−02
244.69	2.29E−02	2.49E−02	1.71E−02
344.27	6.38E−01	7.80E−01	6.99E−01
411.11	6.63E−03	8.44E−03	4.38E−03
443.98	2.24E−02	2.68E−02	2.52E−02
778.89	1.02E+00	1.14E+00	4.47E−01
867.32	1.40E−01	1.68E−01	1.15E−01
964.01	1.99E+00	2.19E+00	1.22E+00
1085.78	1.87E+00	1.70E+00	7.64E−01
1112.02	2.24E+00	2.35E+00	1.37E+00
1212.80	3.06E−02	2.94E−02	8.29E−03
1407.95	8.37E+00	8.59E+00	8.52E+00

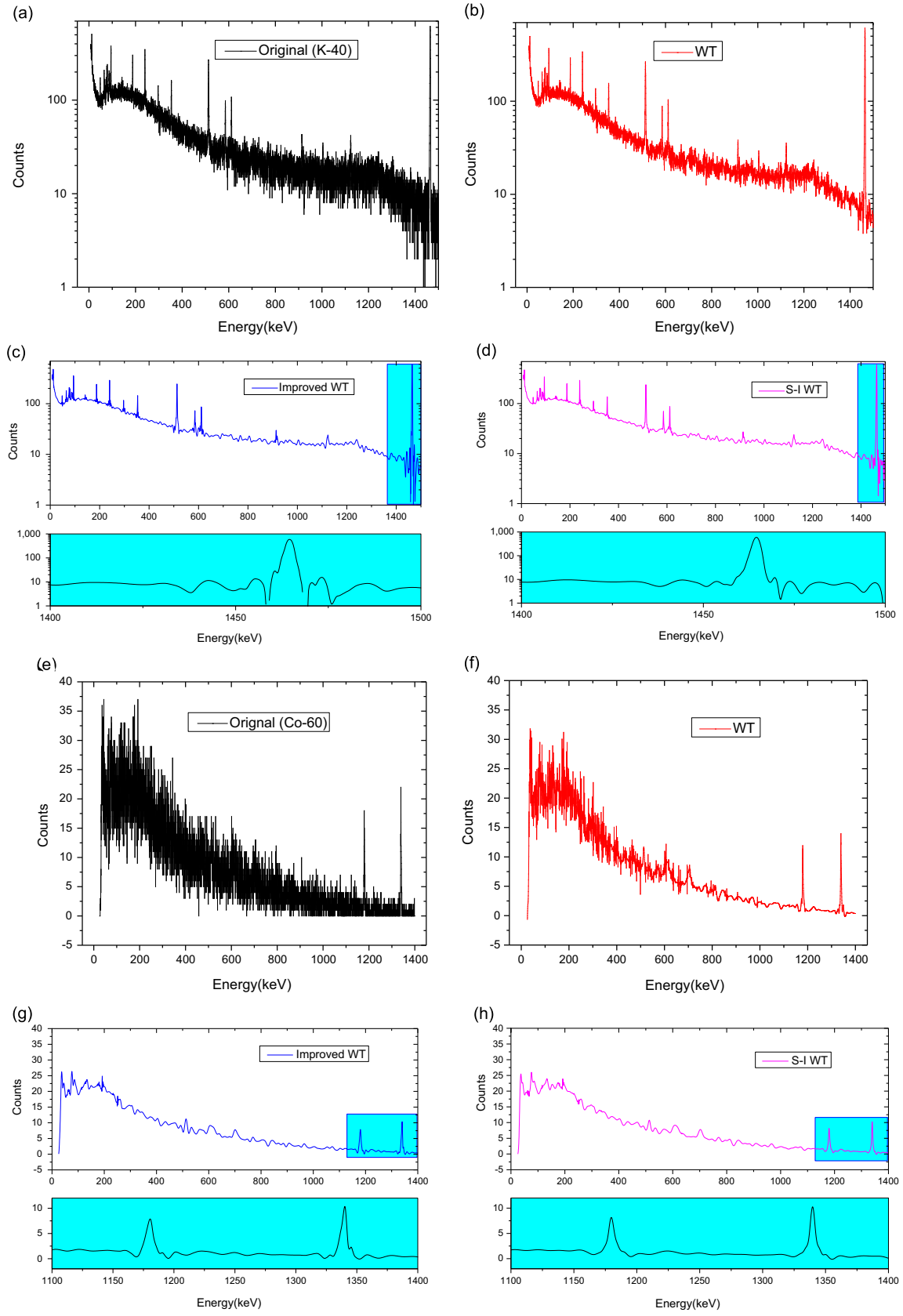

Fig. 5. The noise-suppressed spectrum of Fig. 2(c, d), (a) the original spectrum of K-40, (b) the noise-suppressed K-40 spectrum by WT method, (c) the noise-suppressed K-40 spectrum by improved WT method, (d) the noise-suppressed K-40 spectrum by improved S-I-WT method, (e) the original spectrum of Co-60, (f) the noise-suppressed Co-60 spectrum by improved WT method, (g) the noise-suppressed Co-60 spectrum by improved WT method, (h) the noise-suppressed Co-60 spectrum by improved S-I-WT method.

method had good versatility and enriched the range of application, which made up for the lack of data in Fig. 2.

Fig. 5 presents the de-noised spectra (original spectra are shown in Fig. 2(c) and (d)) with 3 variations of WT. As shown in Fig. 5, S-I WT and improved WT de-noising achieved good results.

4. Conclusion

Based on the preprocessing of the gamma-ray spectrum measured by the SGS system, and using the improved wavelet transform and shift invariant wavelet transform, we obtained smallest attenuation coefficient relative errors with the peak area and significantly reduced statistical fluctuations compared with traditional methods. Given the total measurement time limits in the segmented gamma scanning measurement system, it is necessary to quickly obtain small gamma statistical fluctuations in the spectra. The algorithm not only enhances the figure of merit of the high-resolution gamma-ray spectroscopy, but also is anticipated to be appropriate for straightforward automated quantitative analysis.

Acknowledgement

This research was supported by the National Natural Science Foundation of China (NSFC) (No. 41227802), the Sichuan Province Science Supporting Program Foundation (No. 2014GZ0184), and the Research Funding of Southwest University of Science and Technology (Nos. 13zx7135, 14tdhk03 and 15yyhk14).

References

[1] A. Hernandez-Prieto, B. Quintana, IEEE Transactions on Nuclear Science 60 (2013) 4719.
[2] N. Qian, T. Krings, E. Mauerhofer, et al., Journal of Radioanalytical and Nuclear Chemistry 292 (2012) 1325.
[3] T. Krings, E. Mauerhofer, Applied Radiation and Isotopes 69 (2011) 880–889.
[4] A. Hernandez-Prieto, B. Quintana, Advancements in Nuclear Instrumentation Measurement Methods and their Applications, 2, 2011, pp. 1–5.
[5] R. Venkataraman, M. Villani, S. Croft, et al., Nuclear Instruments and Methods in Physics Research Section A: Accelerators, Spectrometers, Detectors and Associated Equipment 579 (2007) 375.
[6] A.G. Espartero, G. Pina, Nuclear Instruments and Methods in Physics Research Section A: Accelerators, Spectrometers, Detectors and Associated Equipment 422 (1999) 790.
[7] L.S. Saltykov, S.V. Shevchenko, V.I. Slisenko, et al., Practice Periodical of Hazardous, Toxic, and Radioactive Waste Management, (2009) 205.
[8] Zhang Quanhu, China Institute of Atomic Energy 37 (2003) 101.
[9] Yan Xuekun, Liu Mingjian, Zhang Na, et al., Atomic Energy Science and Technology 41 (2007) 505.
[10] Yang Yigang, Wang Ruzhan, Li Yuanjing, Nuclear Technology 25 (2002) 241.
[11] C. Tsabaris, A. Prospathopoulos, Applied Radiation and Isotopes 69 (2011) 1546.
[12] C.J. Sullivan, S.E. Garner, K.B. Blagoev, et al., Nuclear Instruments and Methods in Physics Research Section A: Accelerators, Spectrometers, Detectors and Associated Equipment 579 (2007) 275.
[13] N.G. Kingsbury, Philosophical Transactions of the Royal Society A 9 (1999) 2543.
[14] J.-L. Starck, E.J. Candes, D.L. Donoho, IEEE Transactions on Image Processing 11 (2002) 670.
[15] Thierry Blu, Florian Luisier, IEEE Transactions on image processing 16 (2007) 2778.
[16] Y. Xinge, et al., Optical Engineering 47 (2008) 107002.
[17] J.F. Pang, Gamma Energy Spectroscopy Analysis 3 (1990) 681.
[18] J.F. Pang, Gamma Energy Spectroscopy Analysis 3 (1990) 367.
[19] D.L. Donoho, IEEE Transactions on Information Theory 41 (1995) 613.
[20] W. Wei, Z. Yingtang, R. Guoquan, Chinese Journal of Scientific Instrument 30 (2009) 526.
[21] C. Tie, Z. Jie, Control and Decision 21 (2006) 217.
[22] X. Huang, M. Tan, H. Wu, et al., Procedia Engineering 29 (2012) 1963.
[23] A. Barri, A. Dooms, P. Schelkens, Journal of Mathematical Analysis and Applications 389 (2012) 1303.